Composite Structures 160 (2017) 335–348

Contents lists available at ScienceDirect

Composite Structures

journal homepage: www.elsevier.com/locate/compstruct

An equivalent continuum multiscale formulation for 2D geometrical nonlinear analysis of lattice truss structure

Hui Liu [a,*], Jun Lv [b]

[a] Department of Engineering Mechanics, School of Civil Engineering, Wuhan University, Wuhan, PR China
[b] School of Aeronautics and Astronautics, State Key Laboratory of Structural Analysis for Industrial Equipment, Dalian University of Technology, Dalian, PR China

ARTICLE INFO

Article history:
Received 15 April 2016
Revised 19 September 2016
Accepted 18 October 2016
Available online 18 October 2016

Keywords:
Lattice truss material
Numerical interpolation function
Multiscale finite element method
Geometrical nonlinear analysis
Co-rotational formulation

ABSTRACT

In this work, an equivalent continuum multiscale formulation is presented for the geometrical nonlinear analysis of the structures with lattice truss materials. This formulation is established by combining the extended multiscale finite element method and the co-rotational approach. Firstly, the lattice truss unit cell is equivalent to a continuum coarse element by using a numerical constructed interpolation function in the local coordinate system. Then the tangent stiffness matrix of this coarse element is derived by employing the basic idea of the co-rotational approach in the global coordinate system. Thus, the global nonlinear equilibrium equations of the structure at the macroscopic level can be solved by using the general displacement control algorithm to capture the equilibrium path with multiple critical points. After performing all of the incremental steps and the iterative steps on the macroscopic scale, the microscopic information, such as the displacement, stress and strain, can be obtained easily by virtue of the aforeconstructed numerical interpolation functions once again. In addition, several numerical examples are carried out to study the effects of the layout and size of unit cell, investigate the sensitivity of coarse-scale meshes and verify the validation and efficiency of the presented multiscale formulation.

1. Introduction

Over the past few decades, the lightweight materials and structures are more and more applied in the aerospace industries and civil engineering areas with the development of manufacturing technologies [1,2]. As a kind of lightweight materials, lattice truss materials (as shown in Fig. 1) have received considerable attention due to their inherent advantages [3–5], such as high stiffness/strength-weight ratio [6]. As a result of the rapid development of three-dimensional printing and material preparation technologies, the construction of lattice truss materials and structures become much easier in recent years [7–11]. A lattice can be constructed by a large periodic truss bar with pin-jointed nodes. The lattice structures can be assembled by many periodic unit cells which are composed of some elementary truss bars. This type of structure has lower mass and higher rigidity than traditional ones. Such structures have been widely applied in civil engineering and they also have great potential to construct the ultra-large space structures.

The finite element method (FEM) is usually employed to analyze the problems of such lattice structures. However, these lattice structures usually have multiscale features, i.e., the minimum characteristic size of the lattice truss material is much smaller than the macroscopic size of the lattice structure. This is to say that each lattice structure contains numerous elementary truss bars. Therefore, lots of computational resources will be consumed when using the traditional FEM to solve the problems of lattice structures. What's worse is that the FEM will be failure to do this for some ultra-large lattice structures due to the limitations of the computer capability and CPU time. To solve this problem, many continuum models were developed since the lattices look like continuum media when they become large [13–15]. Moreau and Caillerie [15] developed a continuum model based on the homogenization method for 2D large displacement analysis of lattice truss structure. Tollenaere and Caillerie [16] studied a two-dimensional quasi-periodic lattice truss structure and presented a continuous model derived from the periodic continuous medium homogenization. Burgardt and Cartraud [17] provided a general approach to determine the equivalent beam properties of beam-like lattice trusses based on the energy equivalence. Elsayed and Pasini [18] investigated the structural design of the microscopic lattice

* Corresponding author.
E-mail address: h.liu@whu.edu.cn (H. Liu).

http://dx.doi.org/10.1016/j.compstruct.2016.10.072
0263-8223/

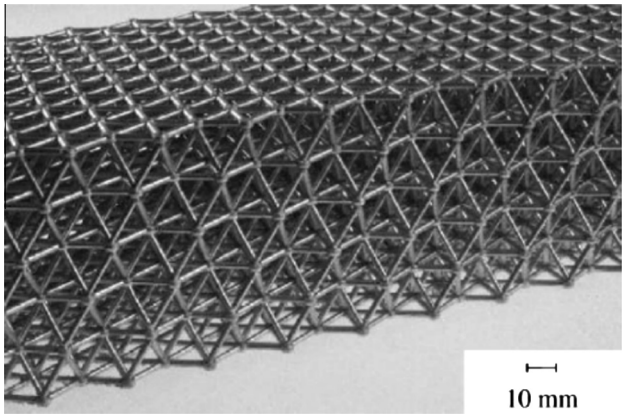

Fig. 1. Photograph of the lattice truss material [12].

architecture with octet-truss cell and the multiscale design of an axially loaded member manufactured of this type of cellular solid.

In this paper, an alternative equivalent continuum model, based on the extended multiscale finite element method (EMsFEM) [19–21] and the co-rotational formulation of geometrical nonlinear problems [22–24], is developed to analyze the geometrical nonlinear problem of lattice truss structure. The EMsFEM was firstly employed to solve the problems of heterogeneous materials in computational solid field by Zhang and his co-workers. This multiscale method has been successfully applied in simulating the linear and nonlinear problems of heterogeneous solid materials [25–27], the mechanical behaviors of bionic nastic materials [28,29], the thermo-mechanical coupling problems of multiphase solid materials [30,31] and the consolidation behaviors of saturated porous media [32,33]. The basic idea of this method is to construct multiscale base functions on the sub-grid domain. These functions can capture and bring the microscopic material information to the macroscopic scale for reducing the overall computational cost efficiently and significantly. In addition, a downscaling computation technique is also proposed for recovering the microscopic results of sub grids from the macroscopic scale solutions of overall coarse-scale mesh. On the other hand, the co-rotational formulation [34–36], as one of common existing formulations to solve the geometrically nonlinear problems [37], is developed for the equivalent coarse-scale continuum element in this work. Within this co-rotational formulation, there are two sets of coordinate systems: local and global ones. The local framework is fixed on the coarse-scale continuum element and moves with the rigid body translation and rotation of this element, while as the global one is fixed and unchanged all the time during the whole deformation processes of structure. This co-rotational formulation divides the whole movement of a finite element into two parts, where one is the rigid body translation and rotation while the other one is the deformation in the local coordinate system. After obtaining the multiscale base functions by the EMsFEM in the local coordinate system, the periodic lattice truss unit cells can be equivalent to a continuum element, whose effective local stiffness matrix and external load vector will be calculated easily and naturally by using the above-mentioned multiscale base functions. Then the tangent stiffness matrix and internal force vector of each equivalent continuum element can be obtained in the global coordinate system via the co-rotational formulation. Thus the global tangent stiffness and external load vector of the equivalent coarse-scale mesh of whole structure can also be assembled naturally. After that, the equilibrium iterative processes for each load incremental step will be performed to find the complex load-displacement equilibrium path by employing the frequently used iteration control algorithms [38], such as the arc-length control methods (ALCM), the generalized displacement control method (GDCM), the work control method (WCM) and the orthogonal residual procedure (ORP). Due to the excellent merit at capturing complex nonlinear behavior at both load and displacement limit points, the GDCM is employed in present work. Finally, the desired microscopic results of any truss element within the unit cell can be recovered easily via the downscaling calculation. To verify the validation and effectiveness of this proposed method, some typical numerical examples are investigated by using both this equivalent multiscale continuum method on the coarse-scale mesh and the traditional FEM on the full-scale mesh.

2. Briefly review of the EMsFEM

In EMsFEM, the bridge between microscopic and macroscopic levels is built through a multiscale shape function, which is usually obtained by solving a boundary value problem on a unit cell domain numerically. Then, the microscopic material properties could be captured and brought to the macroscopic scale for reducing the computational cost significantly. After the macroscopic calculation, the constructed multiscale shape function could be used once again to get the microscopic deformation information of each unit cell. As shown in Fig. 2, both the upscaling and downscaling computation processes can be achieved by virtue of the above-mentioned multiscale shape function.

3. Macroscopic equivalent quantities of the lattice truss unit cell

Generally speaking, three kinds of boundary condition (BC) can be employed for constructing the numerical multiscale shape function, i.e., linear, periodic and oversampling oscillating BCs, which are usually effective for homogeneous, periodic and completely heterogeneous materials, respectively. In this work, the periodic BC is adopted since only the periodic microscopic truss unit cells are taken into account.

The periodic BC is illustrated in Fig. 3, where two corresponding microscopic nodes located on two opposite edges of the unit cell are bound by the relative displacements Δu and Δv in x and y directions, respectively. As an example, to construct the multiscale shape function of macroscopic node 1 in x direction, Δu varies linearly from 1 to 0 along the edge 12 (from the macroscopic node 1–2) and the edge 14. For the other two edges, Δu is set as zero. In addition, another relative displacement Δv is set as zero for all the edges. To avoid the rigid body movement of unit cell, the macroscopic node 3 should be fixed in both x and y directions. After imposing these relative displacement constraints, the multiscale shape function of macroscopic node 1 in x direction can be obtained by solving the static equilibrium equation on the unit cell domain. For more details, one can refer to our previous work [25–33].

The above-constructed multiscale shape function vector of the macroscopic node 1 in the x direction could be denoted as $\boldsymbol{N}_{1x}$, which can be further expressed as

$$\boldsymbol{N}_{1x} = \begin{Bmatrix} \boldsymbol{N}_{1xx} \\ \boldsymbol{N}_{1xy} \end{Bmatrix} \tag{1}$$

where $\boldsymbol{N}_{1xx}$ and $\boldsymbol{N}_{1xy}$ are the components of the vector $\boldsymbol{N}_{1x}$ in x and y directions, respectively. In addition, the dimension of $\boldsymbol{N}_{1x}$ is $2n_s \times 1$ with n_s being the number of microscopic nodes within the unit cell domain. For illustration purpose, $\boldsymbol{N}_{1x}$ is plotted in Fig. 4.

Similarly, the numerical multiscale shape functions of other macroscopic nodes can also be obtained by solving the static equilibrium equations on the unit cell domain with corresponding

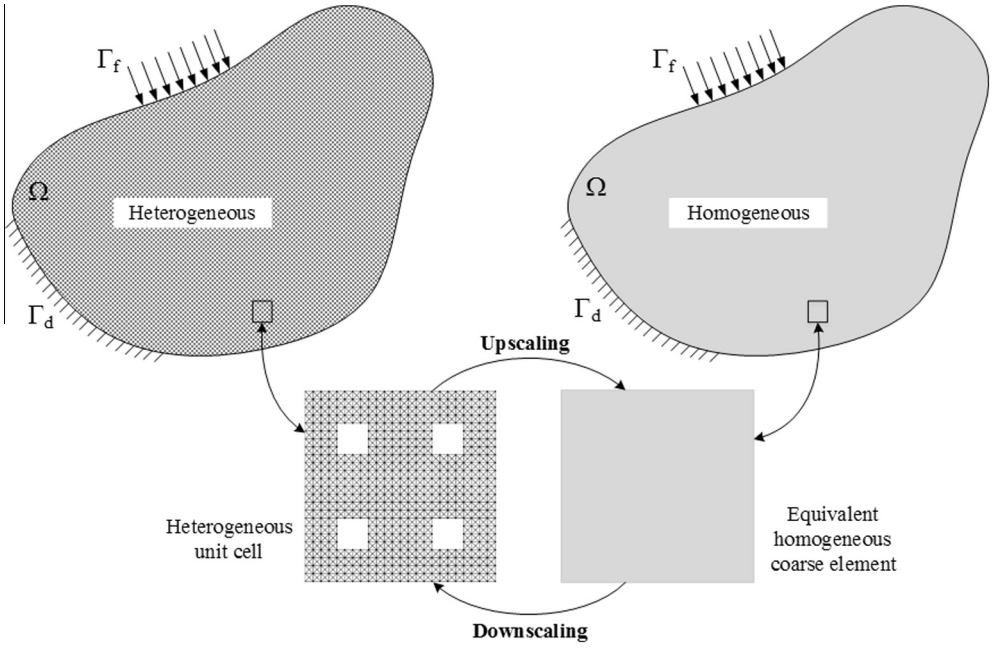

Fig. 2. Schematic description of the EMsFEM.

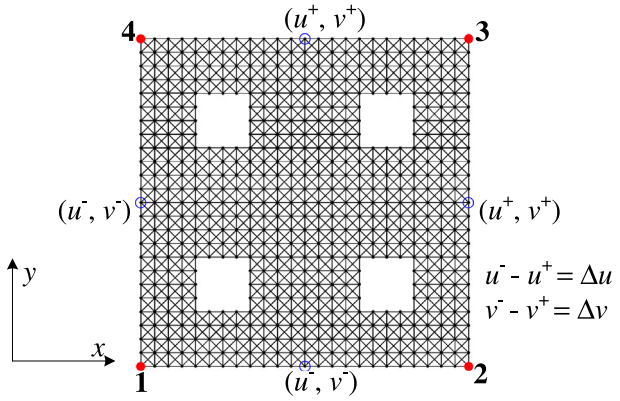

Fig. 3. Illustration of the implementation of the periodic BC.

periodic BCs. Thus, the multiscale shape function matrix $\boldsymbol{N}_E$ of the coarse element could be given as

$$\boldsymbol{N}_E = \begin{bmatrix} \boldsymbol{N}_{1xx} & \boldsymbol{N}_{1yx} & \boldsymbol{N}_{2xx} & \boldsymbol{N}_{2yx} & \boldsymbol{N}_{3xx} & \boldsymbol{N}_{3yx} & \boldsymbol{N}_{4xx} & \boldsymbol{N}_{4yx} \\ \boldsymbol{N}_{1xy} & \boldsymbol{N}_{1yy} & \boldsymbol{N}_{2xy} & \boldsymbol{N}_{2yy} & \boldsymbol{N}_{3xy} & \boldsymbol{N}_{3yy} & \boldsymbol{N}_{4xy} & \boldsymbol{N}_{4yy} \end{bmatrix} \tag{2}$$

where $\boldsymbol{N}_{ixy}$ and $\boldsymbol{N}_{iyx}$ $(i = 1–4)$ represent the additional coupling terms, which can take the Poisson's effect into account effectively and improve the computational accuracy significantly [25–33].

By virtue of the constructed interpolation function of coarse element, the displacement relationship between the macroscopic nodes of coarse element and the corresponding microscopic nodes within the unit cell can be built as

$$\boldsymbol{u}_s = \boldsymbol{N}_E \boldsymbol{U}_E \tag{3}$$

where $\boldsymbol{u}_s$ represents the microscopic displacement vector of the unit cell and $\boldsymbol{U}_E$ is the macroscopic displacement vector of the

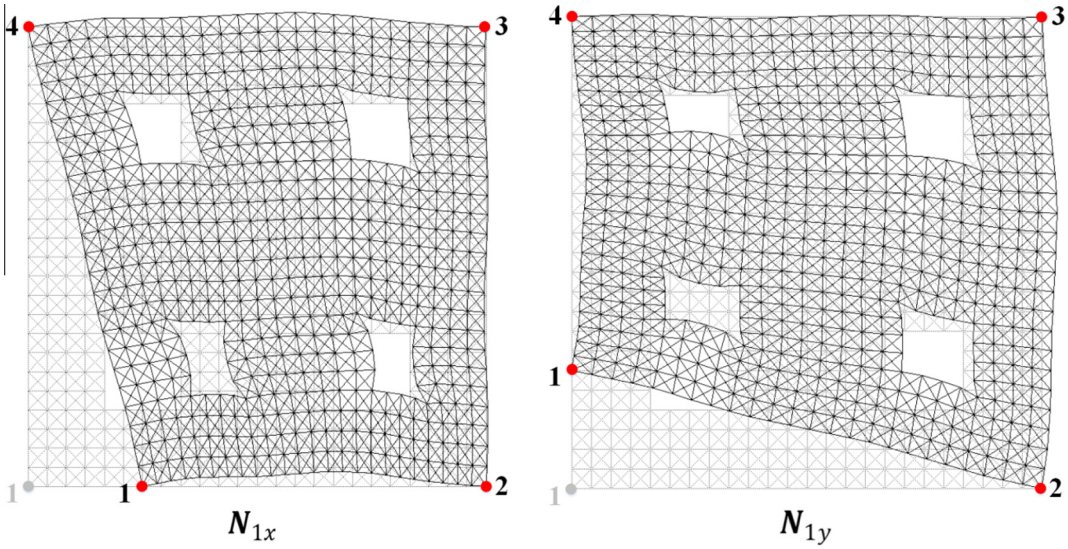

Fig. 4. Illustration of the constructed multiscale shape functions $\boldsymbol{N}_{1x}$ and $\boldsymbol{N}_{1y}$.

coarse element. The dimensions of $\boldsymbol{u}_s$ and $\boldsymbol{U}_E$ are $2n_s \times 1$ and $2n_c \times 1$, respectively, where n_c denotes the number of the macroscopic nodes of one single coarse element. In this paper, we have $n_c = 4$ for two-dimensional problems. It should be mentioned that we usually have $n_s \gg n_c$.

As well known, the static equilibrium equation in finite element discretization form of the unit cell is given by

$$\boldsymbol{K}_s\boldsymbol{u}_s = \boldsymbol{F}_s \tag{4}$$

where $\boldsymbol{K}_s$ represents the overall stiffness matrix of unit cell and $\boldsymbol{F}_s$ is the external force vector which is applied to the unit cell.

Substituting Eq. (3) into Eq. (4) and pre-multiplying $\boldsymbol{N}_E^{\mathrm{T}}$ on the both sides of Eq. (4) lead to

$$\boldsymbol{K}_E\boldsymbol{U}_E = \boldsymbol{F}_E \tag{5}$$

where $\boldsymbol{K}_E$ and $\boldsymbol{F}_E$ are the equivalent macroscopic stiffness matrix and external force vector of the coarse element corresponding to the unit cell. They could be given by

$$\boldsymbol{K}_E = \boldsymbol{N}_E^{\mathrm{T}}\boldsymbol{K}_s\boldsymbol{N}_E,\ \boldsymbol{F}_E = \boldsymbol{N}_E^{\mathrm{T}}\boldsymbol{F}_s \tag{6}$$

By using the constructed multiscale shape function, the heterogeneous unit cell will be equivalent as a solid coarse element. In addition, it should be mentioned that all the quantities described in this section are derived within the local coordinate frame of coarse element and the superscript '*l*' is omitted for simplicity.

4. Multiscale co-rotational formulation

In order to extend the application fields of the EMsFEM to geometric nonlinear problems, the co-rotational formulation is employed herein. Compared with the typical Total/Updated Lagrangian formulations, the co-rotational approach is particularly effective for the large displacement and small strain analysis [34–37]. Its main idea is to decompose the motion of the element into two parts. One is the rigid body motion in the global coordinate system and the other is the pure deformation in the local coordinate system. In this section, a two-scale geometric nonlinear formulation is proposed by combining the above-mentioned multiscale method and the co-rotational approach. During the derivations of the tangent stiffness matrices of microscopic truss element and macroscopic coarse element, two reference coordinate systems are employed herein. The first one is the global frame labeled by '*X*-*Y*' and the other is the local one labeled by '*x*-*y*'. In addition, note that in this work the variables with superscripts '*g*' and '*l*' represent the quantities described in the global and local systems, respectively.

4.1. Macroscopic nonlinear calculation of the whole structure with coarse-scale mesh

In this developed multiscale approach, the heterogeneous unit cell is equivalent to a homogeneous continuum coarse element. To investigate the large displacement and small strain problems of the structures with lattice truss unit cells, the co-rotational approach is employed herein for calculating the equivalent tangent stiffness matrix of the macroscopic coarse element. The main idea of co-rotational approach is to decompose the motion of structure into two parts. One is the rigid body motion in the global coordinate system and the other is the pure deformation in the local coordinate system. The pure deformation process is based on the small strain assumption. Thus the geometric linear theory can be adopted in the local coordinate system.

In this section, we will derive the tangent stiffness matrix of the equivalent coarse element within the global coordinate frame and present the implementation processes of the whole macroscopic computation as illustrated in Fig. 5. Firstly, the lattice truss unit cell is equivalent to a coarse element by virtue of the constructed multiscale shape function in the local coordinate system; Secondly, the tangent stiffness matrix of the equivalent continuum coarse element can be derived by employing the co-rotational approach and can be assembled to form the overall tangent stiffness matrix of the whole structure meshed by the coarse elements; Then, the solving of the geometric nonlinear equations can be performed on the macroscopic scale which will reduce lots of computation cost; Finally, the stress and strain solutions of each truss element on the fine-scale mesh can also be obtained by using the above-constructed multiscale shape function once again.

In Section 3, the lattice truss unit cell is equivalent to a continuum coarse element by virtue of the constructed multiscale shape function within the local coordinate frame. In the co-rotational approach, two sets of coordinate system are shown in Fig. 5, where the global one is denoted by "*O*-*XY*" and the local one is represented by "*c*-*xy*". In Fig. 5, three configurations labeled by "I", "II" and "III" represent the initial, temporary and current configurations, respectively. From I to II, the coarse element undergoes a rigid body motion which can be described by a translation vector $\boldsymbol{U}_c^g$ and a rotation α. From II to III, a pure deformation occurs in the local coordinate system. The translation vector $\boldsymbol{U}_c^g$ can be expressed as $\boldsymbol{U}_c^g = \{\, U_c^g \quad V_c^g \,\}^{\mathrm{T}}$ with U_c^g and V_c^g are the displacement components in the global *X* and *Y* directions of the centroid of the coarse element, respectively. They can be given by

$$U_c^g = \frac{1}{4}\sum_{i=1}^{4} U_i^g,\ V_c^g = \frac{1}{4}\sum_{i=1}^{4} V_i^g \tag{7}$$

where U_i^g and V_i^g are the global displacement components of the node *i* of the coarse element in the *X* and *Y* directions, respectively.

The nodal displacement vector of the node *i* of the coarse element in the local coordinate system is denoted by $\boldsymbol{U}_i^l = \left\{ U_i^l \quad V_i^l \right\}^{\mathrm{T}}$ where U_i^l and V_i^l can be given by

$$\begin{Bmatrix} U_i^l \\ V_i^l \end{Bmatrix} = \begin{bmatrix} \cos\alpha & \sin\alpha \\ -\sin\alpha & \cos\alpha \end{bmatrix} \begin{Bmatrix} X_i + U_i^g - X_c - U_c^g \\ Y_i + V_i^g - Y_c - V_c^g \end{Bmatrix} - \begin{Bmatrix} x_i \\ y_i \end{Bmatrix} \tag{8}$$

where X_c and Y_c are the global coordinates of the centroid of the coarse element; X_i and Y_i denote the global coordinates of the node *i* of the coarse element; x_i and y_i denote the local coordinates of the node *i* of the coarse element; α is the rotation angle of the coarse element from the state I to II. The value of α can be determined such that the following expression is minimized, i.e.

$$\sum_{i=1}^{4}\left[\left(U_i^l\right)^2 + \left(V_i^l\right)^2\right] \tag{9}$$

Taking the variation respect to α and setting the resulting expression equal to zero lead to

$$\tan\alpha = \frac{\sum_{i=1}^{4}\left[x_i\left(Y_i + V_i^g - Y_c - V_c^g\right) - y_i\left(X_i + U_i^g - X_c - U_c^g\right)\right]}{\sum_{i=1}^{4}\left[x_i\left(X_i + U_i^g - X_c - U_c^g\right) - y_i\left(Y_i + V_i^g - Y_c - V_c^g\right)\right]} \tag{10}$$

From the expression (10), two results can be obtained, i.e., α' and $\alpha' + \pi$. One is corresponding to the minimization and the other gives the maximization. Within the global frame, the variational equation of a single coarse element can be given by

$$\delta\boldsymbol{f}_E^g = \boldsymbol{K}_{Et}^g\delta\boldsymbol{U}_E^g \tag{11}$$

where $\boldsymbol{f}_E^g$ denotes the internal force vector of coarse element; $\boldsymbol{K}_{Et}^g$ is the tangent stiffness matrix of coarse element; $\boldsymbol{U}_E^g$ is the nodal displacement vector of coarse element in the global frame and can be written as

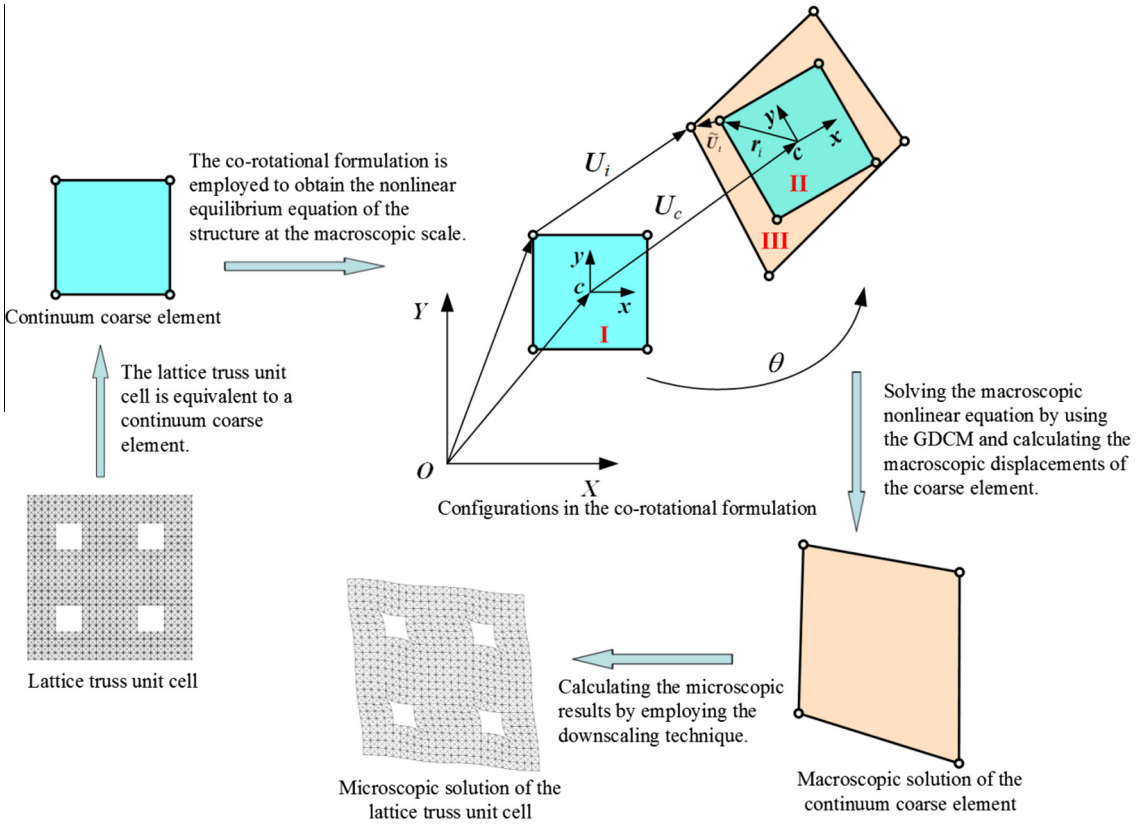

Fig. 5. Illustration of the proposed multiscale co-rotational formulation.

$$\boldsymbol{U}_E^g = \{\, U_1^g \quad V_1^g \quad U_2^g \quad V_2^g \quad U_3^g \quad V_3^g \quad U_4^g \quad V_4^g \,\}^{\mathrm{T}} \tag{12}$$

In addition, we also have

$$\delta(\boldsymbol{U}_E^g)^{\mathrm{T}}\boldsymbol{f}_E^g = \delta\left(\boldsymbol{U}_E^l\right)^{\mathrm{T}}\boldsymbol{f}_E^l \tag{13}$$

$$\delta\boldsymbol{f}_E^l = \boldsymbol{T}_E\delta\boldsymbol{f}_E^g \tag{14}$$

$$\boldsymbol{f}_E^l = \boldsymbol{K}_E^l\boldsymbol{U}_E^l \tag{15}$$

where $\boldsymbol{f}_E^l$ is the internal force vector of coarse element in the local coordinate system; $\boldsymbol{T}_E$ represents a pure rigid body translation matrix; $\boldsymbol{K}_E^l$ is the local stiffness matrix of coarse element, which can be obtained by the first equation in Eq. (6); $\boldsymbol{U}_E^l$ is the nodal displacement vector of coarse element in the local coordinate system, i.e.

$$\boldsymbol{U}_E^l = \left\{\, U_1^l \quad V_1^l \quad U_2^l \quad V_2^l \quad U_3^l \quad V_3^l \quad U_4^l \quad V_4^l \,\right\}^{\mathrm{T}} \tag{16}$$

After some mathematical operations by using these equations, we can have

$$\boldsymbol{U}_E^g = \boldsymbol{T}_E^{\mathrm{T}}\boldsymbol{U}_E^l \tag{17}$$

$$\boldsymbol{K}_{Et}^g = \boldsymbol{K}_{Et1}^g + \boldsymbol{K}_{Et2}^g \tag{18}$$

where $\boldsymbol{K}_{Et1}^g$ can be given by

$$\boldsymbol{K}_{Et1}^g = \boldsymbol{T}_E^{\mathrm{T}}\boldsymbol{K}_E^l\boldsymbol{T}_E \tag{19}$$

in which the translation matrix $\boldsymbol{T}_E$ can be determined by

$$\boldsymbol{T}_E = \boldsymbol{H}\boldsymbol{G}^{\mathrm{T}} \tag{20}$$

with

$$\boldsymbol{G} = diag(\boldsymbol{\Theta},\boldsymbol{\Theta},\boldsymbol{\Theta},\boldsymbol{\Theta}) \text{ with } \boldsymbol{\Theta} = \begin{bmatrix} \cos\alpha & -\sin\alpha \\ \sin\alpha & \cos\alpha \end{bmatrix} \tag{21}$$

$$\boldsymbol{H} = \boldsymbol{I} - \boldsymbol{A}\boldsymbol{B} \tag{22}$$

$$\boldsymbol{A} = \{\, -y_{d1} \quad x_{d1} \quad -y_{d2} \quad x_{d2} \quad -y_{d3} \quad x_{d3} \quad -y_{d4} \quad x_{d4} \,\}^{\mathrm{T}} \tag{23}$$

$$\boldsymbol{B} = \frac{1}{q}\{\, -y_1 \quad x_1 \quad -y_2 \quad x_2 \quad -y_3 \quad x_3 \quad -y_4 \quad x_4 \,\} \tag{24}$$

in which $\boldsymbol{I}$ denotes an identity matrix and the expression of q is $q = \sum_{i=1}^{4}(x_i x_{di} + y_i y_{di})$ where $x_{di} = U_i^l + x_i$ and $y_{di} = V_i^l + y_i$ (i = 1–4).

After some algebraic operations, $\boldsymbol{K}_{Et2}^g$ in Eq. (18) can be given by

$$\boldsymbol{K}_{Et2}^g = \boldsymbol{G}\left(-\boldsymbol{S}^{\mathrm{T}}\boldsymbol{B} - \boldsymbol{B}^{\mathrm{T}}\boldsymbol{S}\boldsymbol{H}\right)\boldsymbol{G}^{\mathrm{T}} \tag{25}$$

with

$$\boldsymbol{H}^{\mathrm{T}}\boldsymbol{f}_E^l = \{\, n_1 \quad n_2 \quad n_3 \quad n_4 \quad n_5 \quad n_6 \quad n_7 \quad n_8 \,\}^{\mathrm{T}} \tag{26}$$

$$\boldsymbol{S} = \{\, n_2 \quad -n_1 \quad n_4 \quad -n_3 \quad n_6 \quad -n_5 \quad n_8 \quad -n_7 \,\} \tag{27}$$

Once we get the equivalent tangent stiffness matrix $\boldsymbol{K}_{Et}^g$ of the coarse element, the overall tangent stiffness matrix $\boldsymbol{K}_{Ct}^g$ of the whole structure with coarse-scale mesh can also be assembled by

$$\boldsymbol{K}_{Ct}^g = \mathrm{A}_{E=1}^{N_E}\left(\boldsymbol{K}_{Et}^g\right) \tag{28}$$

where $\mathrm{A}_{E=1}^{N_E}$ represents the matrix (or vector) assemble operator and N_E denotes the number of the coarse element in the coarse-scale mesh. Similarly, the internal force vector $\boldsymbol{f}_C^g$ and external load vector

$\boldsymbol{F}_C^g$ of the whole structure meshed by the coarse-scale grids can also be assembled as

$$\boldsymbol{f}_C^g = \mathrm{A}_{E=1}^{N_E}(\boldsymbol{f}_E^g),\ \boldsymbol{F}_C^g = \mathrm{A}_{E=1}^{N_E}(\boldsymbol{F}_E^g) \tag{29}$$

where $\boldsymbol{f}_E^g$ and $\boldsymbol{F}_E^g$ can be obtained by $\boldsymbol{f}_E^g = \boldsymbol{T}_E^{\mathrm{T}}\boldsymbol{f}_E^l$ and $\boldsymbol{F}_E^g = \boldsymbol{T}_E^{\mathrm{T}}\boldsymbol{F}_E^l$, respectively, where $\boldsymbol{F}_E^l$ can be calculated according to the second equation in Eq. (6).

After obtaining the tangent stiffness matrix, the internal force vector and the external load vector of the whole structure meshed with the coarse-scale grids in the global coordinate system, the equilibrium iterations during the geometric nonlinear analysis can be performed only on the macroscopic level, which will save lots of computation cost since the nonlinear equations are only solved on the macroscopic scale. Furthermore, the microscopic stress and strain information can be obtained through the down-scaling computation based on the macroscopic displacement solution. In this paper, the generalized displacement control method (GDCM) is employed for solving the macroscopic nonlinear equations with multiple extreme points. The implementation processes are described as follows.

For the kth iteration step of the jth incremental step, the nonlinear equilibrium equation of the structure on the macroscopic scale can be written as

$$(\boldsymbol{K}_{Ct}^g)_{k-1}^j(\Delta\boldsymbol{U}_C^g)_k^j = (\boldsymbol{F}_C^g)_k^j - (\boldsymbol{f}_C^g)_{k-1}^j \tag{30}$$

where $\Delta\boldsymbol{U}_C^g$ represents the incremental displacement vector of the macroscopic nodes on the coarse-scale mesh. The initial values of the quantities in Eq. (30) are set as the convergent values in the last incremental step, i.e., $(\boldsymbol{K}_{Ct}^g)_0^j = (\boldsymbol{K}_{Ct}^g)^{j-1}$, $(\boldsymbol{F}_C^g)_0^j = (\boldsymbol{F}_C^g)^{j-1}$, $(\boldsymbol{f}_C^g)_0^j = (\boldsymbol{f}_C^g)^{j-1}$, $(\boldsymbol{U}_C^g)_0^j = (\boldsymbol{U}_C^g)^{j-1}$.

The external load vector can be rewritten in the incremental form as

$$(\boldsymbol{F}_C^g)_k^j = (\boldsymbol{F}_C^g)_{k-1}^j + (\Delta\boldsymbol{F}_C^g)_k^j \tag{31}$$

Furthermore, the above equation can be rewritten as

$$(\boldsymbol{F}_C^g)_k^j = (\boldsymbol{F}_C^g)_{k-1}^j + \lambda_k^j\widehat{\boldsymbol{F}}_C^g \tag{32}$$

where λ_k^j denotes the incremental loading factor of the kth iteration in the jth incremental step and $\widehat{\boldsymbol{F}}_C^g$ is the reference load vector.

According to Eq. (30), we have

$$(\boldsymbol{K}_{Ct}^g)_{k-1}^j(\Delta\boldsymbol{U}_C^g)_k^j = \lambda_k^j\widehat{\boldsymbol{F}}_C^g + (\boldsymbol{R}_C^g)_{k-1}^j \tag{33}$$

where

$$(\boldsymbol{R}_C^g)_{k-1}^j = (\boldsymbol{F}_C^g)_{k-1}^j - (\boldsymbol{f}_C^g)_{k-1}^j \tag{34}$$

Then, the Eq. (33) can be decomposed into two parts, i.e.

$$(\boldsymbol{K}_{Ct}^g)_{k-1}^j\left(\Delta\widehat{\boldsymbol{U}}_C^g\right)_k^j = \widehat{\boldsymbol{F}}_C^g \tag{35}$$

$$(\boldsymbol{K}_{Ct}^g)_{k-1}^j(\Delta\overline{\boldsymbol{U}}_C^g)_k^j = (\boldsymbol{R}_C^g)_{k-1}^j \tag{36}$$

In this way, the overall incremental displacement can be given by

$$(\Delta\boldsymbol{U}_C^g)_k^j = \lambda_k^j\left(\Delta\widehat{\boldsymbol{U}}_C^g\right)_k^j + (\Delta\overline{\boldsymbol{U}}_C^g)_k^j \tag{37}$$

Thus, the macroscopic overall displacement of the structure can be updated by

$$(\boldsymbol{U}_C^g)_k^j = (\boldsymbol{U}_C^g)_{k-1}^j + (\Delta\boldsymbol{U}_C^g)_k^j \tag{38}$$

Similarly, the total external load can be updated by

$$(\boldsymbol{F}_C^g)_k^j = \Lambda_k^j\widehat{\boldsymbol{F}}_C^g \tag{39}$$

where Λ_k^j is the loading factor, which can be calculated by

$$\Lambda_k^j = \Lambda_{k-1}^j + \lambda_k^j \tag{40}$$

The incremental loading factor λ_k^j is an unknown parameter which should be determined by an additional constraint condition [38]. For the generalized displacement control method (GDCM), λ_k^j can be calculated according to a generalized stiffness parameter (GSP). For the 1st iteration of each incremental step, λ_1^j can be given by

$$\lambda_1^j = \lambda_1^1\sqrt{|GSP|} \tag{41}$$

where λ_1^1 is a given initial incremental loading factor and GSP is defined as

$$GSP = \frac{\left\{\left(\Delta\widehat{\boldsymbol{U}}_C^g\right)_1^1\right\}^{\mathrm{T}}\left\{\left(\Delta\widehat{\boldsymbol{U}}_C^g\right)_1^1\right\}}{\left\{\left(\Delta\widehat{\boldsymbol{U}}_C^g\right)_1^{j-1}\right\}^{\mathrm{T}}\left\{\left(\Delta\widehat{\boldsymbol{U}}_C^g\right)_1^j\right\}} \tag{42}$$

For the kth ($k \geqslant 2$) iteration of each incremental step, λ_k^j will be obtained by

$$\lambda_k^j = \frac{\left\{\left(\Delta\widehat{\boldsymbol{U}}_C^g\right)_1^{j-1}\right\}^{\mathrm{T}}\left\{(\Delta\overline{\boldsymbol{U}}_C^g)_k^j\right\}}{\left\{\left(\Delta\widehat{\boldsymbol{U}}_C^g\right)_1^{j-1}\right\}^{\mathrm{T}}\left\{\left(\Delta\widehat{\boldsymbol{U}}_C^g\right)_k^j\right\}} \tag{43}$$

The implementation processes of the proposed multiscale co-rotational formulation based on the GDCM are introduced in detail as follows and the corresponding flow chart is also given in Fig. 6.

5. Numerical validations

In this section, several numerical examples are carried out to verify the effectiveness of the proposed method and investigate the size effects of the lattice truss microstructures as well as the coarse-scale mesh sensitivity. In the following examples, the 'ECMM' represents the result obtained based on the coarse-scale mesh by using the proposed multiscale formulation, while the 'FEM-F' and 'ANSYS' are the solutions obtained based on the full scale (fine-scale) mesh. Actually, 'FEM-F' is the result computed by combining the traditional FEM and co-rotational approach, while 'ANSYS' denotes the result calculated by the commercial software ANSYS. The co-rotational formulation of 'FEM-F' are given in the appendix. In addition, the parameters employed in these examples are all dimensionless.

Example 1. A cantilever beam (as shown in Fig. 7) subjected a uniform force on its right end is studied to investigate the effect of the number of truss materials within the unit cells and the effect of the coarse-scale mesh sensitivity on the computation results. Two microstructures with different truss distributions and properties are taken into account as shown in Fig. 8, where the Young's moduli of the truss materials in Fig. 8 are all 1.0×10^9 except for the red inclined trusses in Microstructure B. The Young's moduli of the red inclined trusses are 5.0×10^9. The truss cross sectional area is 7.854×10^{-7} in this example. Microstructures A and B represent the homogeneous and heterogeneous unit cells. In this example, we firstly investigated the effect of the unit cells with different number of trusses on the computation results based on a fixed coarse-scale mesh (38×4). Then, we analyzed the coarse-scale mesh sensitivity based on a fixed fine-scale mesh (the num-

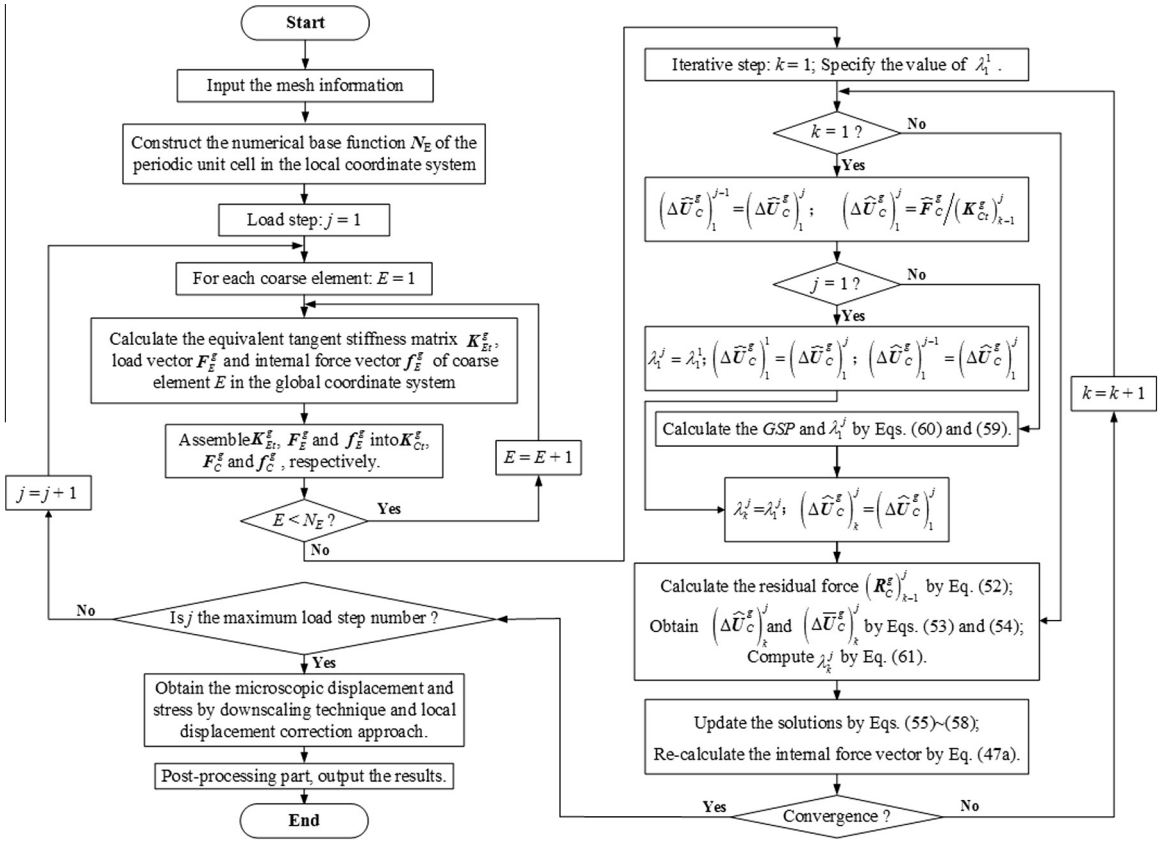

Fig. 6. The flow chart of the proposed multiscale co-rotational formulation.

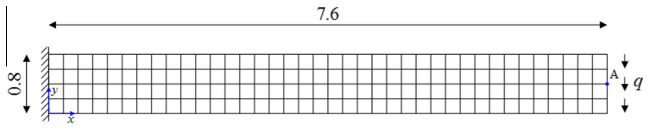

Fig. 7. A cantilever beam with 38×4 coarse elements.

ber of coarse elements is changed and the number of fine elements is unchanged for different sizes of unit cells). It should be mentioned that the external distributed force q is 125 for Microstructure A, while it is set to 100 for Microstructure B.

To investigate the effect of the number of trusses within the unit cells, a 38×4 coarse-scale mesh (Fig. 7) and two microstructures (Fig. 8) with different layouts are taken into account. In this analysis, the reference solutions ('FEM-F' and 'ANSYS') will be different for different kinds of unit cells since the coarse-scale mesh is unchanged (38×4) while the layout of unit cell is changing for different unit cells. Therefore, the fine-scale (full scale) mesh corresponding to each unit cell as shown in Fig. 8 is different. To verify the validation of the proposed method, those results obtained by the proposed multiscale formulation based on the coarse-scale mesh are compared with the reference solutions labeled by 'FEM-F' and 'ANSYS' calculated on the fine-scale mesh. The comparison is plotted in Figs. 9 and 10. One can see that the results obtained by the traditional FEM and co-rotational formulation are exactly the same as those calculated by the commercial software ANSYS. This indicates that the co-rotational formulation of the truss element given in Appendix A is correct. For different unit cells, the multiscale computation results at the load factor $\lambda = 1$ are compared with their corresponding reference ones. Their relative errors of the displacement of Point A in the negative y direction are also plotted in Fig. 11. For Microstructure A, the relative error is slightly reduced from 2% for $n_f = 2$ to 1.7% for $n_f = 16$ (n_f denotes the layout of unit cell as shown in Fig. 8). For Microstructure B, it reduces from 5.4% for $n_f = 2$ to 3.3% for $n_f = 16$. From the results shown in Fig. 11, we can also conclude that: (1) the proposed formulation can obtain enough accurate results by comparison with the reference ones since all of the relative errors are less than about 5%; (2) the selection of the number of trusses within the unit cells has little effect on the computation accuracy for the homogeneous microstructure, which it has significant effect on the computation accuracy for the heterogeneous microstructure; (3) the unit cell with more trusses can improve the corresponding computation accuracy. It should be mentioned that this proposed method is different with the well-known computational homogenization method [39–41], in which there is one key assumption that the governing length scales are well separated, i.e., $\ell_{\text{discrete}} \ll \ell_{\text{micro}} \ll \ell_{\text{macro}}$. However, there is no such an assumption in our proposed multiscale formulation.

On the other hand, to investigate the effects of the coarse-mesh sensitivity and the size selection of unit cell on the computation results based on the same lattice truss structure, the cantilever beam shown in Fig. 7 is re-meshed on the coarse scale. The grids for these different meshes are 304×32, 152×16, 76×8 and 38×4, respectively. Since these coarse-scale meshes are corresponding to a same lattice truss structure, the unit cells for these coarse-scale meshes are also different and they are depicted in Fig. 12, where the unit cells (a), (b), (c) and (d) are corresponding to the aforementioned coarse-scale meshes, respectively. The results obtained by the proposed multiscale formulation based on the four different coarse-scale meshes and their corresponding unit cells are compared with the reference ones based on the full scale mesh (see Figs. 13 and 14). These results indicate that

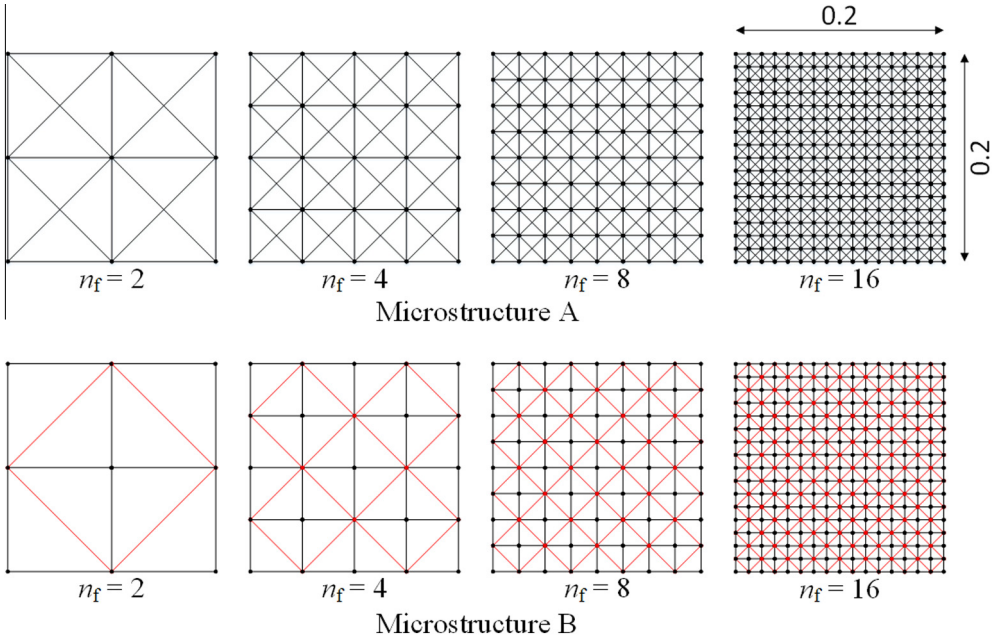

Fig. 8. Two different microstructures.

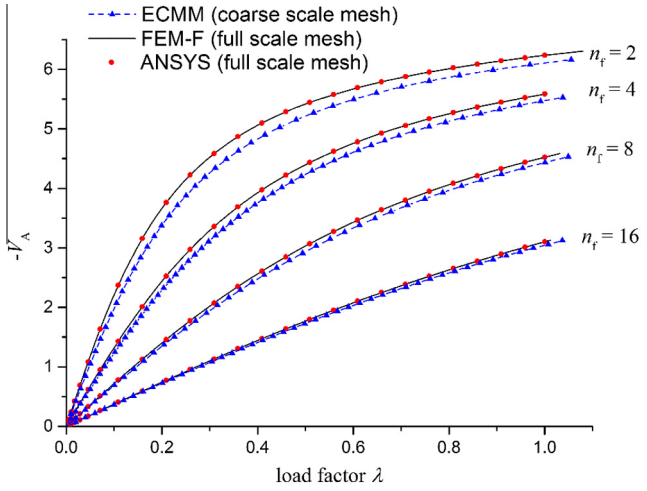

Fig. 9. Comparison of the displacement of Point A in the negative *y* direction for Microstructure A.

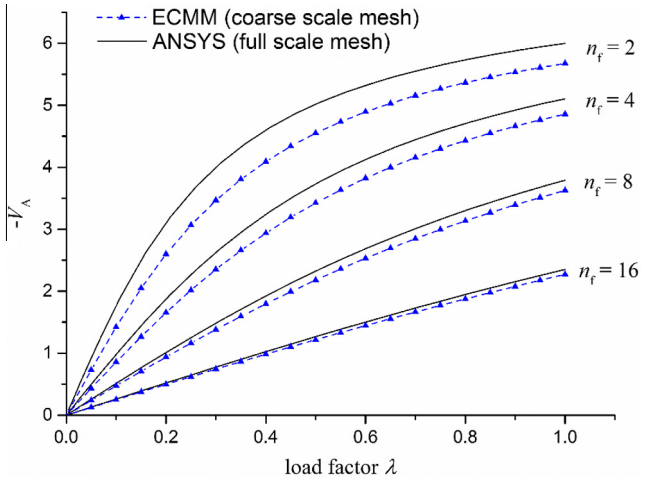

Fig. 10. Comparison of the displacement of Point A in the negative *y* direction for Microstructure B.

increasing the number of the coarse elements will not improve the accuracy of the computation results for a same lattice truss structure, but increasing the size of unit cell will improve it significantly. Furthermore, this conclusion will be also validated by Fig. 15, where the relative error of the displacement of Point A in the negative *x* direction are plotted. With the increase of the size of unit cell, the relative error is significantly reduced from 20.63% to 1.73% for Microstructure A and from 43.6% to 6.7% for Microstructure B. This is to say that increasing the unit cell size can improve the accuracy of computation results obtained by the proposed multiscale formulation. The reason behind this is that the heterogeneity of the unit cell with less trusses is stronger and it is not suitable to be equivalent as a continuum coarse element [25–33].

Example 2. A L-shape frame depicted in Fig. 16 is considered herein to investigate the validation and the computational efficiency of the proposed multiscale method. In this example, the Young's modulus and the cross-sectional area of truss are 1.0×10^6 and 7.854×10^{-7}, respectively. The sizes of the computational model are $L_1 = 2.16$ and $L_2 = 0.24$. The dimension of the unit cell is 0.06×0.06.

The displacement results of Point A in the *x* direction obtained by the proposed method and ANSYS are plotted in Fig. 17, from which we can see that these two results agree very well. The displacement of Point A in the *x* direction at $q = 0.5$ is 1.622 for the multiscale solution 'ECMM' and it's 1.637 for the reference result 'ANSYS'. The relative error between them is about 0.92%, which indicates that the proposed multiscale method can provide high accuracy results by comparison with the reference one. In addition, Table 1 is listed to show the high computation efficiency of the proposed formulation. From the data in the table, we can see that there are 115 and 41 load steps for the solutions 'ECMM' and 'ANSYS', respectively. While their computation time are 17 s and 1579 s. Then the average computation time for each load step for these two approaches are about 0.15 s and 38.51 s. This is to say that more than 99% of the computation time for each load step

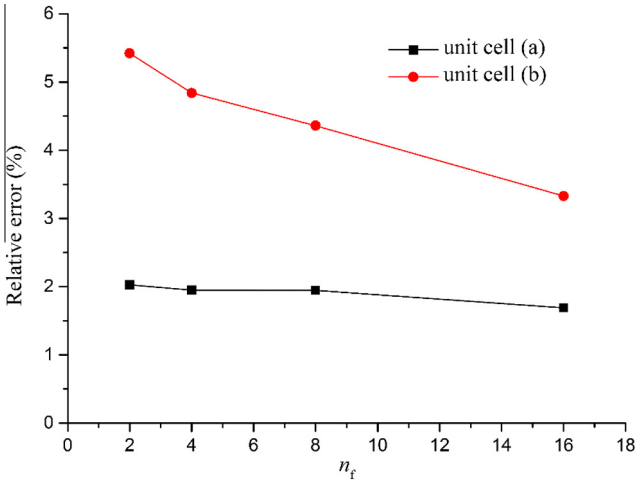

Fig. 11. Relative error of the displacement of Point A in the y direction with increasing the number of trusses in the unit cell.

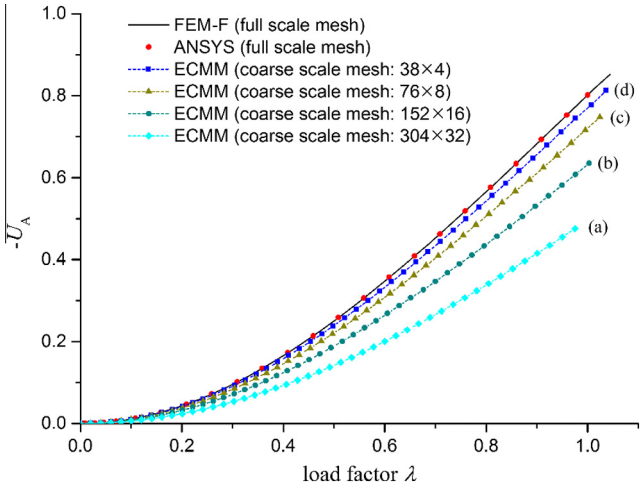

Fig. 13. Comparison of the displacement of Point A in the negative x direction for the structure with different coarse-scale meshes for Microstructure A.

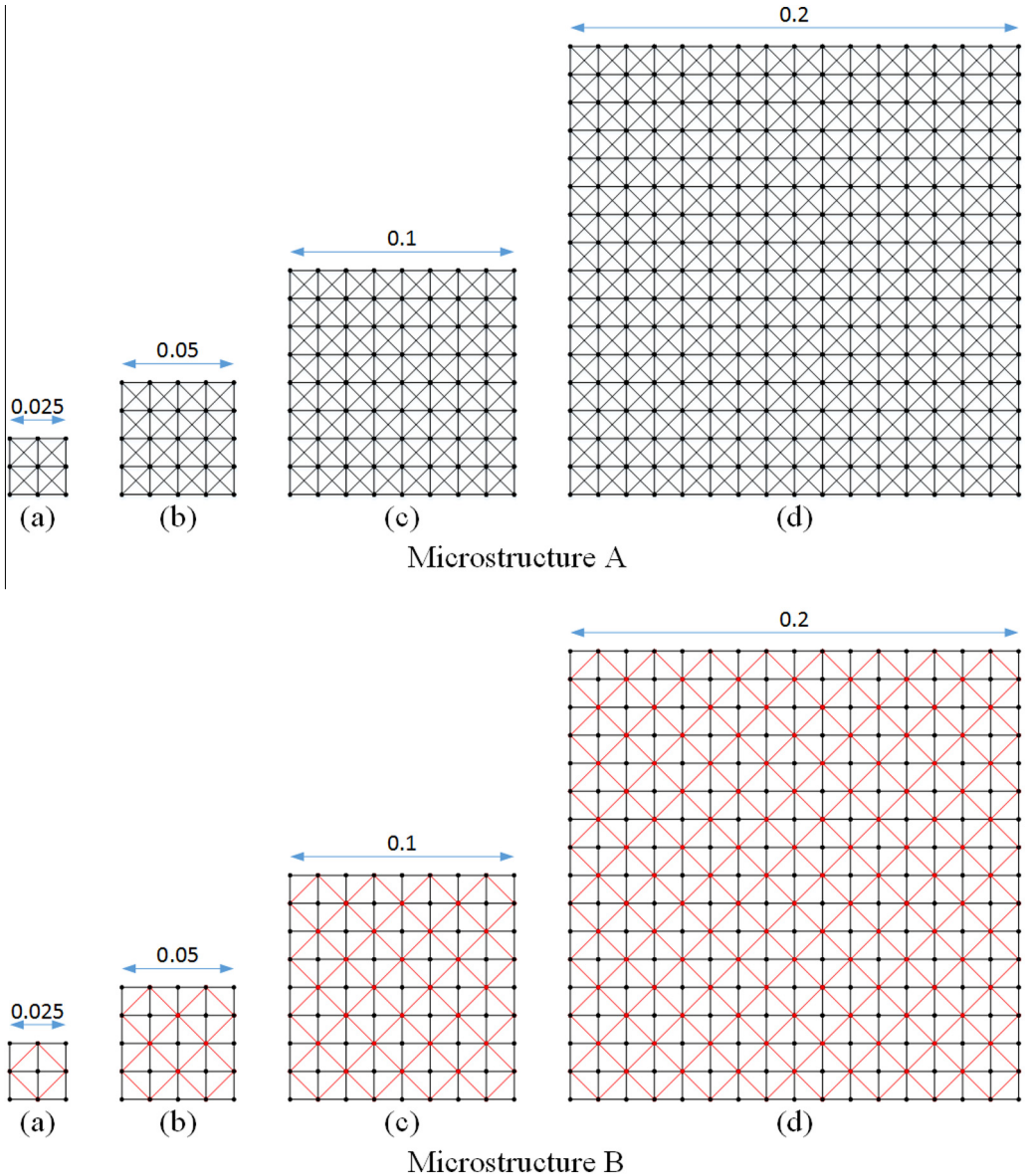

Fig. 12. Four unit cells for Microstructures A and B.

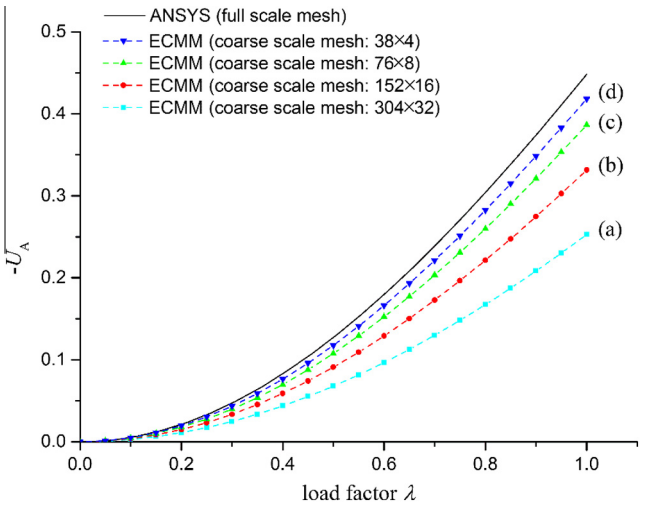

Fig. 14. Comparison of the displacement of Point A in the negative x direction for the structure with different coarse-scale meshes for Microstructure B.

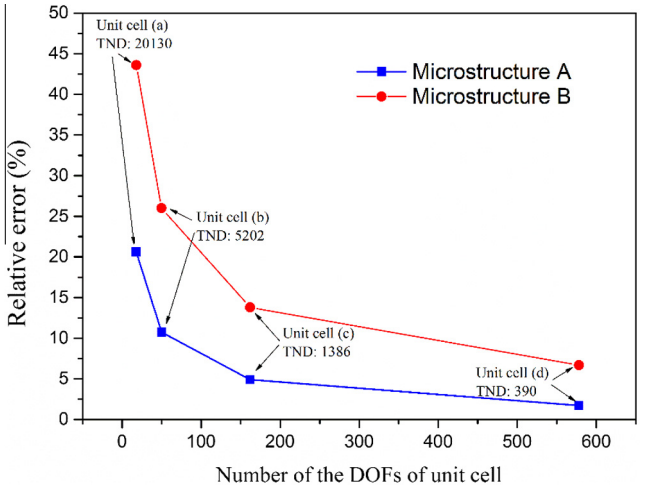

Fig. 15. The variation of the relative error of the displacement of Point A in the negative x direction with the increase of the number of DOFs of unit cell (TND shown in the figure represents the total number of the DOFs of the corresponding coarse-scale mesh).

can be saved by employing the proposed multiscale co-rotational formulation.

Example 3. In this example, the structural instability analysis [42,43] will be investigated by using the proposed multiscale formulation. A Γ-shape structure with two kinds of unit cells is carried out to verify the validation and efficiency of the proposed method for the geometrical nonlinear problem with multiple critical points. The computational model is depicted in Fig. 18, where q is a uniform external force and the dimensions of unit cells are 0.12×0.12. In unit cell (a), all of the trusses have the same properties, i.e., Young's modulus and the cross-sectional area are 1.0×10^9 and 7.854×10^{-7}, respectively. In unit cell (b), the properties of the black thin trusses are the same as those in unit cell (a), while the Young's modulus and the cross-sectional area of the red thick trusses are 5.0×10^9 and 7.854×10^{-7} respectively.

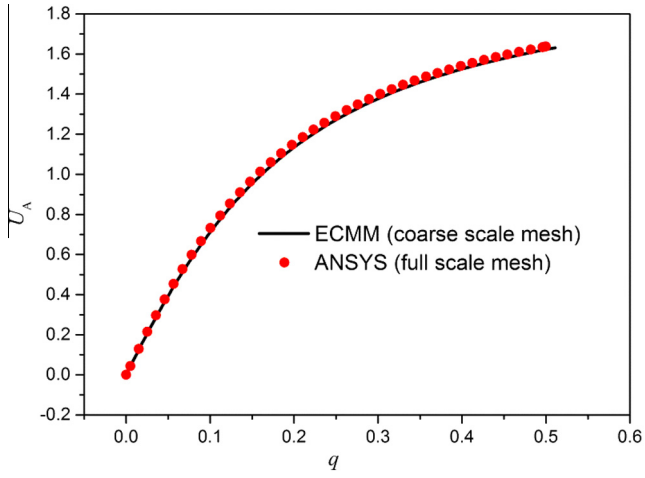

Fig. 17. Comparison of the displacement of Point A in the x direction.

Table 1
Comparison of the computational efficiency for the L-shape frame.

	Number of Total DOFs	Number of Load Steps	CPU time
ECMM	770	115	17 s
ANSYS	332,162	41	1579 s

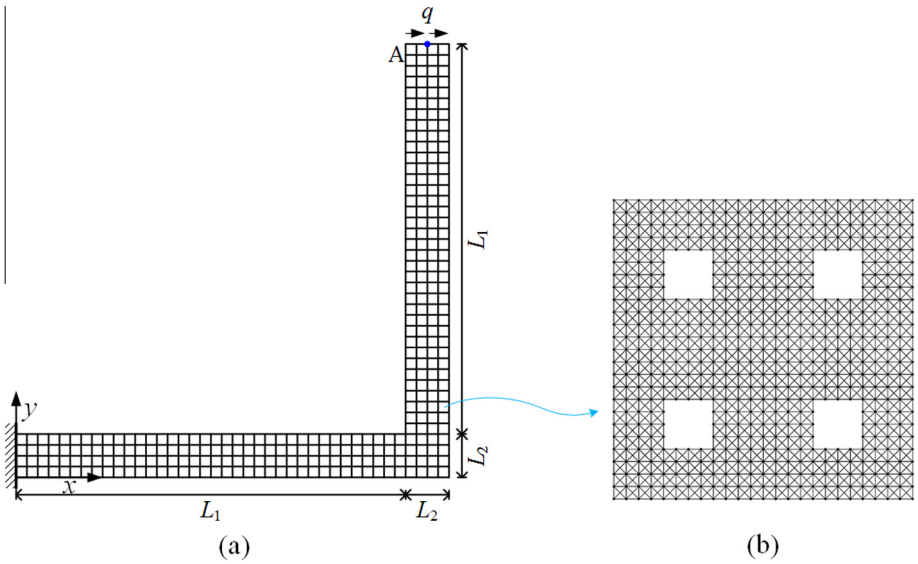

Fig. 16. Computational model: (a) L-shape frame with the coarse-scale mesh and its boundary conditions; (b) Unit cell.

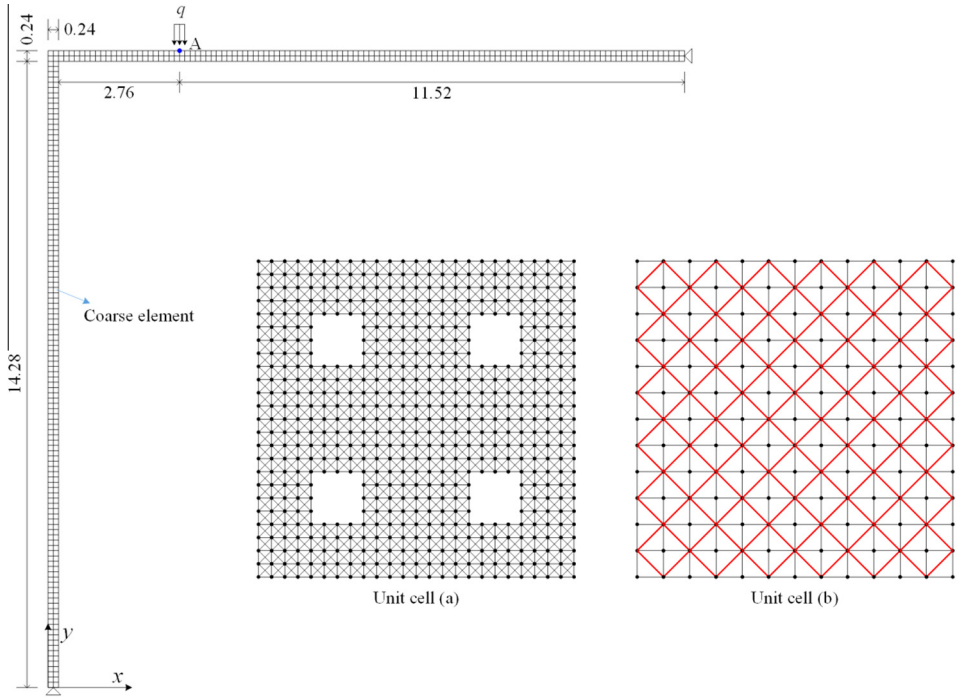

Fig. 18. Γ-shape structure and the unit cells.

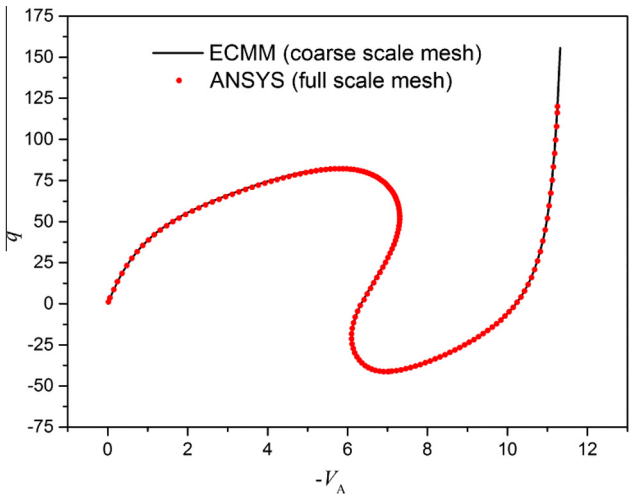

Fig. 19. Load-displacement curve of the structure with unit cell (a).

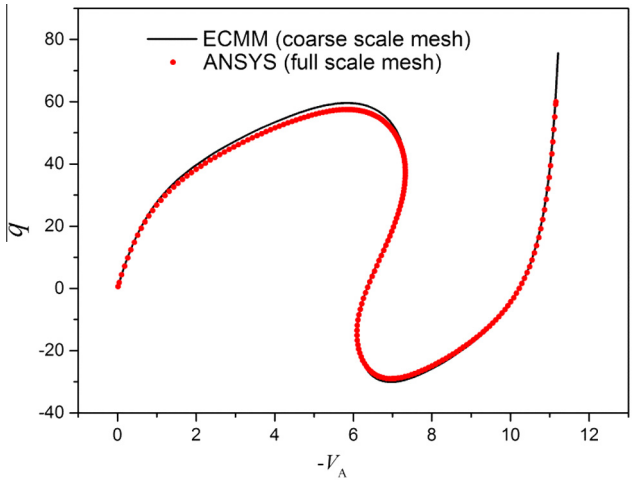

Fig. 20. Load-displacement curve of the structure with unit cell (b).

The equilibrium paths of the structures with two different unit cells are depicted in Figs. 19 and 20, from which we can observe that the paths have multiple critical points and the results calculated by the proposed method based on the coarse-scale mesh is quite consistent with those computed by ANSYS based on the full scale mesh. This verifies the validation of the presented multiscale formulation. In addition, for the structure with unit cell (a), the uniform distributed forces q at the first inflection point are 82.83 and 82.16 for the proposed multiscale solution 'ECMM' and the reference result 'ANSYS', respectively. The relative error between them is about 0.81%. For the structure with unit cell (b), they are 59.61 and 57.48 for the results 'ECMM' and 'ANSYS', respectively. Correspondingly, the relative error is about 3.71%, which is much higher than that for the structure with unit cell (a). The reason behind this can be found from the size effect analysis in Example 1, where the proposed multiscale formulation will provide more accuracy results when the unit cell has higher density of the truss. Furthermore, in order to study the computational efficiency of the presented method, the comparison of the computation cost is shown in the Table 2, from which we can conclude that the presented formulation has a high efficiency. The reason behind this has been mentioned above, i.e., the material microscopic properties are captured and brought to the macroscopic scale by virtue of the numerically constructed base functions easily and then the original nonlinear problems can be solved on the macroscopic scale. Moreover, all the iteration computation can be performed only on the macroscopic scale (coarse-scale mesh), which will save lots of computational cost. After obtaining the convergent macroscopic computation result, the microscopic information can also be retrieved by virtue of the constructed multiscale base functions easily.

Table 2
Comparison of the computational efficiency of the Γ-shape structure.

Unit cells	Methods	Number of Total DOFs	Number of Load Steps	CPU time
(a)	ECMM	1446	2060	270 s
	ANSYS	530,018	161	17,408 s
(b)	ECMM	1446	1860	262 s
	ANSYS	144,050	221	4781 s

6. Conclusions

In this work, an equivalent continuum multiscale method (ECMM) is developed by combining the extended multiscale finite element method (EMsFEM) and the co-rotational formulation for the geometrical nonlinear analysis of the structures with lattice truss unit cells. Firstly, the basic ideas of the EMsFEM is briefly reviewed. Then, the macroscopic equivalent quantities in the local system of the unit cell are determined. Next, the co-rotational formulation is adopted to obtain the tangent stiffness matrix in the global system of the equivalent continuum coarse element and the overall tangent stiffness matrix of the structure at the macroscopic level in the global system could be assembled naturally. Finally, the nonlinear equilibrium equations of the structure at the macroscopic level can be solved by employing the general displacement control method and the results of each microscopic node and truss element within the unit cell can also be calculated easily by using the downscaling computation.

Several numerical examples were implemented to investigate the layouts and the size effects of unit cell. The results indicated that the effects of different unit cell layouts on the computation accuracy are not obvious for the case with fixed coarse-scale mesh. However, increasing the unit cell size will improve the accuracy significantly for the case with fixed fine-scale mesh. Furthermore, the validation and efficiency of the proposed multiscale formulation were also investigated by comparison with the results of the traditional FEM and ANSYS on the fine-scale mesh.

Acknowledgement

The supports of the National Natural Science Foundation of China (11402178, 11302040), the China Postdoctoral Science Foundation (2014M552078, 2015T80831, 2014T70244), the Fundamental Research Funds for the Central Universities (DUT15RC(4)39), and the Hubei Provincial Natural Science Foundation (2014CFB336) are gratefully acknowledged.

Appendix A. Co-rotational formulation of 2D truss element

The description of 2D truss element configurations is shown in Fig. A1, where the movement of truss element is divided into two parts, i.e., firstly the truss element moves to a temporary configuration from the initial one through a rigid body motion and then the truss element undergoes a pure deformation from the temporary configuration to the current one. During the pure deformation processing, the geometric linear theory could be employed to describe the movement of the truss element in the local coordinate system. Thus, the stress-strain relationship of truss element can be given by

$$\sigma^l = E\varepsilon^l \tag{A1}$$

where σ and ε are the stress and strain of the plane two-node truss element, respectively. E denotes the Young's modulus of the truss element and the superscript 'l' represents the local system. The strain ε^l can be expressed as

$$\varepsilon^l = \frac{u_2^l - u_1^l}{l_0} \tag{A2}$$

where u_i^l (i = 1–2) represents the nodal displacement of the truss element described in the local system and l_0 denotes the length of truss element. For convenience, Eq. (A2) can be rewritten in the matrix form as

$$\varepsilon^l = \frac{1}{l_0}(\boldsymbol{c}^l)^{\mathrm{T}}\boldsymbol{u}^l \tag{A3}$$

with

$$\boldsymbol{c}^l = \{-1 \quad 1 \quad 0 \quad 0\}^{\mathrm{T}},\ \boldsymbol{u}^l = \{u_1^l \quad u_2^l \quad v_1^l \quad v_2^l\}^{\mathrm{T}} \tag{A4}$$

The internal force vector $\boldsymbol{f}_i^l$ in the local frame can be given by

$$\boldsymbol{f}_i^l = A_0 E\varepsilon^l \boldsymbol{c}^l \tag{A5}$$

where A_0 represents the cross section of the truss element.

By virtue of the transformation matrix $\boldsymbol{T}$ between the local and global frames, the global internal force vector $\boldsymbol{f}_i^g$ and nodal displacement vector $\boldsymbol{u}^g$ can be obtained by

$$\boldsymbol{f}_i^g = \boldsymbol{T}^{\mathrm{T}}\boldsymbol{f}_i^l,\ \boldsymbol{u}^g = \boldsymbol{T}^{\mathrm{T}}\boldsymbol{u}^l \tag{A6}$$

where

$$\boldsymbol{T} = \begin{bmatrix} \cos\theta & 0 & \sin\theta & 0 \\ 0 & \cos\theta & 0 & \sin\theta \\ -\sin\theta & 0 & \cos\theta & 0 \\ 0 & -\sin\theta & 0 & \cos\theta \end{bmatrix} \tag{A7}$$

According to Eq. (A6), we have

$$\delta\boldsymbol{f}_i^g = \boldsymbol{T}^{\mathrm{T}}\delta\boldsymbol{f}_i^l + \delta\boldsymbol{T}^{\mathrm{T}}\boldsymbol{f}_i^l \tag{A8}$$

By using Eq. (A5), the expression of $\delta\boldsymbol{f}_i^l$ can be obtained as

$$\delta\boldsymbol{f}_i^l = \frac{\partial\boldsymbol{f}_i^l}{\partial\boldsymbol{u}^l}\delta\boldsymbol{u}^l = \boldsymbol{K}^l\delta\boldsymbol{u}^l \tag{A9}$$

where $\boldsymbol{K}^l$ denotes the stiffness matrix of truss element in the local coordinate system and can be written as

$$\boldsymbol{K}^l = \frac{1}{l_0}EA_0(\boldsymbol{c}^l)(\boldsymbol{c}^l)^{\mathrm{T}} \tag{A10}$$

Substituting the relation $\delta\boldsymbol{u}^l = \boldsymbol{T}\delta\boldsymbol{u}^g$ into Eq. (A9) and the first term of the right hand side of Eq. (A8) results in

$$\boldsymbol{T}^{\mathrm{T}}\delta\boldsymbol{f}_i^l = \boldsymbol{T}^{\mathrm{T}}\boldsymbol{K}^l\boldsymbol{T}\delta\boldsymbol{u}^g = \boldsymbol{K}_1^g\delta\boldsymbol{u}^g \tag{A11}$$

where $\boldsymbol{K}_1^g$ is the first part of the tangent stiffness matrix of truss element and can be given as $\boldsymbol{K}_1^g = \boldsymbol{T}^{\mathrm{T}}\boldsymbol{K}^l\boldsymbol{T}$.

In the second part of the right hand side of Eq. (A8), $\delta\boldsymbol{T}^{\mathrm{T}}$ can be given by

$$\delta\boldsymbol{T}^{\mathrm{T}} = \begin{bmatrix} -\sin\theta & 0 & -\cos\theta & 0 \\ 0 & -\sin\theta & 0 & -\cos\theta \\ \cos\theta & 0 & -\sin\theta & 0 \\ 0 & \cos\theta & 0 & -\sin\theta \end{bmatrix}\delta\theta \tag{A12}$$

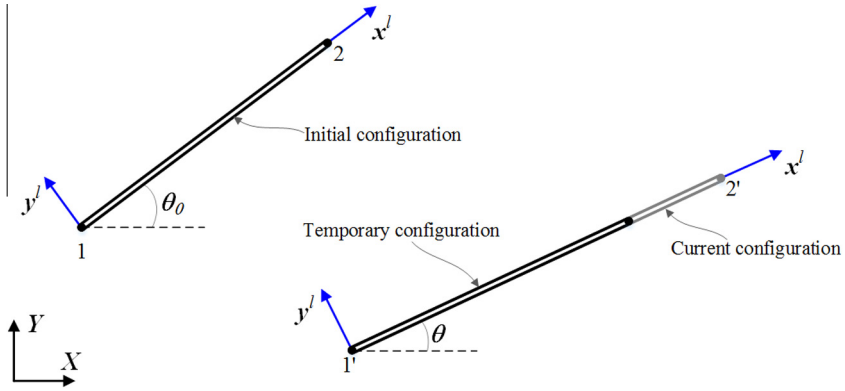

Fig. A1. Description of the movement of truss element.

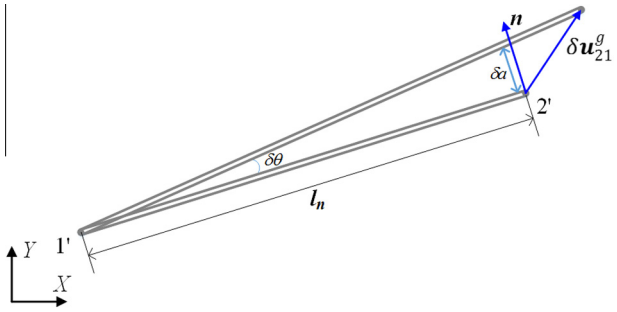

Fig. A2. Illustration of $\delta\theta$.

where $\delta\theta$, illustrated in Fig. A2, denotes a small angle change of the truss element in the current configuration.

The normal vector of the truss element in the current configuration could be written as

$$\boldsymbol{n} = \frac{1}{l_n}\{-y'_{21} \quad x'_{21}\}^{\mathrm{T}} \tag{A13}$$

where $y'_{21} = y'_2 - y'_1$ and $x'_{21} = x'_2 - x'_1$ with (x'_i, y'_i) being the global nodal coordinates of the truss element in the current configuration. l_n is the length of the truss element in the current configuration.

Since $\delta\theta$ is an infinitesimal quantity, $\delta\theta$ can be obtained by

$$\delta\theta = \delta a / l_n = \left(\boldsymbol{n}^{\mathrm{T}}\delta\boldsymbol{u}^g_{21}\right)/l_n = \left(\boldsymbol{y}^{\mathrm{T}}_{21}\delta\boldsymbol{u}^g\right)/\left(l_n^2\right) \tag{A14}$$

where the meaning of δa is depicted in Fig. A2; $\delta\boldsymbol{u}^g_{21}$ and $\boldsymbol{y}^{\mathrm{T}}_{21}$ are expressed as

$$\delta\boldsymbol{u}^g_{21} = \{\delta u^g_{21} \quad \delta v^g_{21}\}^{\mathrm{T}},\ \boldsymbol{y}_{21} = \{y'_{21} \quad -y'_{21} \quad x'_{21} \quad -x'_{21}\}^{\mathrm{T}} \tag{A15}$$

with $u^g_{21} = u^g_2 - u^g_1$ and $v^g_{21} = v^g_2 - v^g_1$.

Substituting Eqs. (A5), (A12) and (A14) into the second part of the right hand side of Eq. (A8) leads to

$$\delta\boldsymbol{T}^{\mathrm{T}}\boldsymbol{f}^l_i = \frac{A_0 E\varepsilon^l}{l_n^2}\begin{bmatrix} -\sin\theta & 0 & -\cos\theta & 0 \\ 0 & -\sin\theta & 0 & -\cos\theta \\ \cos\theta & 0 & -\sin\theta & 0 \\ 0 & \cos\theta & 0 & -\sin\theta \end{bmatrix} \boldsymbol{c}^l\boldsymbol{y}^{\mathrm{T}}_{21}\delta\boldsymbol{u}^g = \boldsymbol{K}^g_2\delta\boldsymbol{u}^g \tag{A16}$$

According to the geometric relationship of the truss element in the current configuration, the expressions of $\sin\theta$ and $\cos\theta$ can be easily obtained. After some basic algebraic operations, the second part of the tangent stiffness matrix of truss element can be given by

$$\boldsymbol{K}^g_2 = \frac{A_0 E\varepsilon^l}{l_n^3}\begin{bmatrix} (y'_{21})^2 & -(y'_{21})^2 & -x'_{21}y'_{21} & x'_{21}y'_{21} \\ -(y'_{21})^2 & (y'_{21})^2 & x'_{21}y'_{21} & -x'_{21}y'_{21} \\ -x'_{21}y'_{21} & x'_{21}y'_{21} & (x'_{21})^2 & -(x'_{21})^2 \\ x'_{21}y'_{21} & -x'_{21}y'_{21} & -(x'_{21})^2 & (x'_{21})^2 \end{bmatrix} \tag{A17}$$

By substituting Eqs. (A11) and (A16) into Eq. (A8), we have

$$\delta\boldsymbol{f}^g_i = \boldsymbol{T}^{\mathrm{T}}\delta\boldsymbol{f}^l_i + \delta\boldsymbol{T}^{\mathrm{T}}\boldsymbol{f}^l_i = \left(\boldsymbol{K}^g_1 + \boldsymbol{K}^g_2\right)\delta\boldsymbol{u}^g = \boldsymbol{K}^g_t\delta\boldsymbol{u}^g \tag{A18}$$

where $\boldsymbol{K}^g_t$ is the tangent stiffness matrix of the truss element and can be given by $\boldsymbol{K}^g_t = \boldsymbol{K}^g_1 + \boldsymbol{K}^g_2$.

After obtaining the tangent stiffness matrix of the truss element, the above co-rotational formulation can be performed based on the fine-scale mesh and the resulting solution will be seen as the reference solution for comparison purpose.

References

[1] Chung D. Composite materials: science and applications. second ed. Springer; 2010.
[2] Immarigeon J-P, Holt RT, Koul AK, et al. Lightweight materials for aircraft applications. Mater Charact 1995;35:41–67.
[3] Xiong J, Mines R, Ghosh R, et al. Advanced micro-lattice materials. Adv Eng Mater 2015. doi: http://dx.doi.org/10.1002/adem.201400471.
[4] Ashby MF, Evans A, Fleck NA, et al. Metal foams: a design guide. Woburn, MA: Butterworth-Heinemann; 2000.
[5] Meza LR, Das S, Greer JR. Strong, lightweight, and recoverable three-dimensional ceramic nanolattices. Science 2014;345:1322–6.
[6] Deshpande VS, Ashby MF, Fleck NA. Foam topology: bending versus stretching dominated architectures. Acta Mater 2001;49:1035–40.
[7] Zhong L, Li X. Simulation analysis of lightweight cylindrical lattice materials with different unit cells. J Coastal Res 2015;73:155–9.
[8] Wallach JC, Gibson LJ. Mechanical behavior of a three-dimensional truss material. Int J Solids Struct 2001;38:7181–96.
[9] Cao X, Hua H. Acoustic responses of the composite sandwich plates with lattice truss core to the subsonic turbulent boundary layer. Compos Struct 2016;153:176–92.
[10] Wu Q, Ma L, Wu L, Xiong J. A novel strengthening method for carbon fiber composite lattice truss structures. Compos Struct 2016;153:585–92.
[11] Jin M, Hu Y, Wang B. Compressive and bending behaviours of wood-based two-dimensional lattice truss core sandwich structures. Compos Struct 2015;124:337–44.
[12] Deshpande VS, Fleck NA, Ashby MF. Effective properties of the octet-truss lattice material. J Mech Phys Solids 2001;49:1747–69.
[13] Noor AK. Continuum modeling for repetitive lattice structures. Appl Mech Rev 1988;41(7):285–96.
[14] Nayfeh AH, Hefzy MS. Continuum modeling of three-dimensional truss-like space structures. AIAA J 1978;16(8):779–87.
[15] Moreau G, Caillerie D. Continuum modeling of lattice structures in large displacement applications to buckling analysis. Comput Struct 1998;68:181–9.
[16] Tollenaere H, Caillerie D. Continuous modeling of lattice structures by homogenization. Adv Eng Softw 1998;29:699–705.
[17] Burgardt B, Cartraud P. Continuum modeling of beamlike lattice trusses using average methods. Comput Struct 1999;73:267–79.
[18] Elsayed MSA, Pasini D. Multiscale structural design of columns made of regular octet-truss lattice material. Int J Solids Struct 2010;47:1764–74.

[19] Zhang HW, Wu JK, Lv J, et al. Extended multiscale finite element method for mechanical analysis of heterogeneous materials. Acta Mech Sin 2010;26:899–920.
[20] Zhang HW, Liu H, Wu JK. A uniform multiscale method for 2D static and dynamic analyses of heterogeneous materials. Int J Numer Meth Eng 2013;94:714–46.
[21] Zhang HW, Wu JK, Fu ZD. Extended multiscale finite element method for elasto-plastic analysis of 2D periodic lattice truss materials. Comput Mech 2010;45:623–35.
[22] Crisfield MA. A consistent co-rotational formulation for non-linear, three-dimensional, beam-elements. Comput Methods Appl Mech Eng 1990;81(2):131–50.
[23] Crisfield MA, Moita GF. A unified co-rotational framework for solids, shells and beams. Int J Solids Struct 1996;33(20–22):2969–92.
[24] Moita GF, Crisfield MA. A finite element formulation for 3-D continua using the co-rotational technique. Int J Numer Meth Eng 1996;39(22):3775–92.
[25] Zhang HW, Liu Y, Zhang S, et al. Extended multiscale finite element method: its basis and applications for mechanical analysis of heterogeneous materials. Comput Mech 2014;53(4):659–85.
[26] Zhang HW, Liu H, Wu JK. A uniform multiscale method for 2D static and dynamic analyses of heterogeneous materials. Int J Numer Meth Eng 2013;93:714–46.
[27] Liu H, Zhang HW. A uniform multiscale method for 3D static and dynamic analyses of heterogeneous materials. Comput Mater Sci 2013;79:159–73.
[28] Zhang HW, Lv J. A multiscale method for the numerical analysis of active response characterization of 3D nastic structures. Smart Mater Struct 2012;21:085009.
[29] Lv J, Liu H, Zhang HW. A multiscale co-rotational method for geometrically nonlinear shape morphing of 2D fluid actuated cellular structures. Mech Mater 2014;79:1–14.
[30] Zhang S, Yang DS, Zhang HW, et al. Coupling extended multiscale finite element method for thermoelastic analysis of heterogeneous multiphase materials. Comput Struct 2013;121:32–49.
[31] Zhang HW, Yang DS, Zhang S, et al. Multiscale nonlinear thermoelastic analysis of heterogeneous multiphase materials with temperature-dependent properties. Finite Elem Anal Des 2014;88:97–117.
[32] Zhang HW, Fu ZD, Wu JK. Coupling multiscale finite element method for consolidation analysis of heterogeneous saturated porous media. Adv Water Resour 2009;32:268–79.
[33] Zhang HW, Lu MK, Zheng YG, et al. General coupling extended multiscale FEM for elasto-plastic consolidation analysis of heterogeneous saturated porous media. Int J Numer Anal Meth Geomech 2015;39(1):63–95.
[34] Crisfield MA, Moita GF. A unified co-rotational framework for solids, shells and beams. Int J Solids Struct 1996;33:2969–92.
[35] Felippa CA, Haugen B. A unified formulation of small-strain corotational finite elements: I. Theory. Comput Methods Appl Mech Eng 2005;194:2285–335.
[36] Battini JM. A non-linear corotational 4-node plane element. Mech Res Commun 2008;35(6):408–13.
[37] Urthaler Y, Reddy JN. A corotational finite element formulation for the analysis of planar beams. Commun Numer Methods Eng 2005;21:553–70.
[38] Leon SE, Paulino GH, Pereira A, et al. A unified library of nonlinear solution schemes. Appl Mech Rev 2011;64:040803.
[39] Kouznetsova VG, Geers MGD, Brekelmans WAM. Multi-scale second-order computational homogenization of multi-phase materials: a nested finite element solution strategy. Comput Methods Appl Mech Eng 2004;193:5525–50.
[40] Geers MGD, Kouznetsova VG, Brekelmans WAM. Multi-scale computational homogenization: trends and challenges. J Comput Appl Math. 2010;234:2175–82.
[41] Coenen EWC, Kouznetsova VG, Geers MGD. Multi-scale continuous-discontinuous frame work for computational-homogenization-localization. J Mech Phys Solids 2012;60:1486–507.
[42] Triantafyllidis N. Puckering instability phenomena in the hemispherical cup test. J Mech Phys Solids 1985;33(2):117–9. 121-139.
[43] Geymonat G, Muller S, Triantafyllidis N. Homogenization of nonlinearly elastic materials, microscopic bifurcation and macroscopic loss of rank-one convexity. Arch Ration Mech Anal 1993;122:231–90.